Molecular "Wiring" Glucose Oxidase in Supramolecular Architecture

Liu Deng, Ying Liu, Guocheng Yang, Li Shang, Dan Wen, Fuan Wang, Zhiai Xu, and Shaojun Dong*

State Key Laboratory of Electroanalytical Chemistry, Changchun Institute of Applied Chemistry, Chinese Academy of Sciences, Changchun, Jilin 130022, People's Republic of China

Received November 1, 2006; Revised Manuscript Received March 14, 2007

Supramolecular organized multilayers were constructed by multiwalled carbon nanotubes modified with ferrocene-derivatized poly(allylamine) redox polymer and glucose oxidase by electrostatic self-assembly. From the analysis of voltammetric signals and fluorescence results, a linear increment of the coverage of enzyme per bilayer was estimated, which demonstrated that the multilayer is constructed in a spatially ordered manner. The cyclic voltammograms obtained from the indium tin oxide (ITO) electrodes coated by the $(Fc\text{-}PAH@CNT/GOx)_n$ multilayers revealed that bioelectrocatalytic response is directly correlated to the number of deposited bilayers; that is, the sensitivity is tunable by controlling the number of bilayers associated with ITO electrodes. The incorporation of redox-polymer-functionalized carbon nanotubes (CNT) into enzyme films resulted in a 6−10-fold increase in the glucose electrocatalytic current; the bimolecular rate constant of $FADH_2$ oxidation (wiring efficiency) was increased up to 12-fold. Impedance spectroscopy data have yielded the electron diffusion coefficient (D_e) of this nanostructure to be over 10^{-8} cm^2 s^{-1}, which is typically higher than those systems without CNT by at least a factor of 10, indicating that electron transport in the new supramolecular architecture was enhanced by communication of the redox active site of enzyme, redox polymer, and CNT.

1. Introduction

The use of redox enzymes in integrated chemical systems has enabled the design of devices capable of molecular recognition.[1] The electrical signal triggered by the enzyme can be integrated into circuits leading to biosensors, miniaturized labs-on-chips, bimolecular microelectronics, or biofuel cells.[2] Electrical communication between redox enzymes and electrode surfaces represents the basic process to activate redox-active biocatalysts.[3] Redox sites in proteins, however, lack direct electrical contact with electrodes due to the insulation of the redox center by the protein. So the architecture of integrated enzyme and electron mediator has important advantages in bioelectronic and biosensor technology.[4−11] Films including enzymes and redox polymer "wires" in their structure allow high selectivity toward molecular recognition and electrical communication in a single sensing device.[5−7] Electron transfer occurs when the tethered redox centers of the polymer collide with the redox centers of the immobilized enzymes. In general, these sensors exhibit high current densities and have been reported to be greater than 1 mA cm^{-2} in some cases. Furthermore, a recent study had reported that the incorporation of single-walled carbon nanotubes into a redox polymer−enzyme hydrogel led to a dramatic increase in the sensor output.[6] A redox hydrogel of this type not only provides a very suitable environment for enzyme entrapment but also allows electrochemical oxidation of the redox prosthetic flavin adenine dinucleotide group of glucose oxidase and the electrode by a diffusion-like electron-hopping mechanism mediated by the redox groups attached to the polymer backbone. It is worthwhile noticing that in the hydrogel there is a random distribution of components with little control over the molecular orientation while spatially ordered enzyme assemblies built with the same active components of the hydrogel offer several advantages over a random polymer.[7] An alternative approach is to use the step-by-step electrostatic self-assembly between a charged surface and oppositely charged molecules in solution first introduced by Decher[8] with molecular-level control that offers the possibility of the preparation of a supported organized supramolecular system. The formation of such systems, which facilitate directional electron transfer, has proved invaluable to the advancement of biosensors for genomic treatment and the development of biofuel cells.[5,8−11] The first effective electrical wiring of GOx in a self-assembled organized layer-by-layer (LbL) multilayer with a ferrocene redox polymer (Fc-PAH) acting as a molecular wire has been described by Calvo et al.[5] They reported a similar osmium complex derivatized by poly(allylamine) (Os-PAH) and GOx deposited stepwise in similar alternate polymer enzyme multilayer.[8−11] The specific rate of bimolecular $FADH_2$ oxidation (wiring efficiency) is limited by the diffusion-like electron-hopping mechanism in the multilayers.[11] Carbon nanotubes (CNTs)have been used widely in the fabrication of electrochemical sensing devices and biosensors during the past decade because they can promote electron transfer of some electroactive substances.[12] This has led more recently to an upsurge of research on incorporating CNTs into enzyme-based biosensing platforms. Some of the electrode configurations employing carbon nanotubes that have been developed include the following: (a) physically adsorbed onto the nanotubes in solution then casting nanotubes onto electrodes,[13] (b) microfabrication of nanoelectrode ensembles and arrays by either adsorbing the enzyme or first immobilizing its flavin adenine dinucleotide (FAD) center onto single-walled carbon nanotubes (SWNTs) and then reconstituting the enzyme,[14] (c) entrapped the enzyme on CNT by electropolymerization,[15] or (d) assembled enzyme on multiwalled carbon

* Author to whom correspondence should be addressed. Phone: +86-431-5262101. Fax: +86-431-5689711. E-mail: dongsj@ciac.jl.cn.

10.1021/bm061049l CCC: $37.00
Published on Web 06/12/2007

nanotubes (MWNTs) wrapped by polyelectrolyte.[16] The polymer-wrapped MWNT/GOx multilayer composite for biosensing applications was demonstrated as a new way to the introduction of CNTs into biologically relevant systems.

In this paper, we have demonstrated a more generalized approach by which enzymes are immobilized in redox-polymer-modified CNTs. Glucose oxidase is multilayered and immobilized on a negatively charged indium tin oxide (ITO) surface by LbL assembly of GOx and Fc-PAH-modified CNTs. So the aim of the construction of a reagentless enzyme biosensor is achieved. The resulting electrode shows a porous structure and exhibits excellent bioelectrocatalytic response to the oxidation of glucose and very effective electrochemical communication between the successive layers. We have studied the propagation of charge within the resulting structures and the enzyme catalysis; quantitative determination of the enzyme electrical "wiring efficiency", kinetic coefficients of the reactions involved, and the effect of the number of adsorbed layers can be evaluated. To our knowledge, this is the first report of the incorporation of MWNTs into redox polymer−enzyme films via electrostatic self-assembly.

2. Experimental Section

2.1. Reagents. The glucose oxidase (E.C. 1.1.3.4), FAD, and PAH were obtained from Sigma Chemical Co. And ferrocene carboxaldehyde was obtained from Aldrich Chemical Co. They were used as received without further purification. Standard solutions of FAD for the fluorescence studies were prepared by dilution of their stock solution with 0.05 M phosphate buffer.

MWNTs (95%, 20−50 nm) purchased from Shenzhen Nanotech. Port. Co. Ltd. (Shenzhen, China) were first shortened and functionalized by sonicating in a mixture of concentrated HNO_3 and H_2SO_4 (1:3, v/v) for 6 h followed by extensive washing in deionized water until the filtrate was neutral. Then the pH was adjusted to 8.0 to achieve net negatively charged carboxylate anions. The negatively charged CNTs were centrifuged at 10 000 rpm for 30 min to remove the supernatant and dried in a vacuum. Glucose was purchased from Beijing Chemical Reagents (Beijing, China), and the stock solution of glucose was allowed to mutorotate at room temperature overnight before use. All other chemicals were of analytical grade. Approximately 10 mM phosphate-buffered saline (PBS) solutions, consisting of Na_2HPO_4 and NaH_2PO_4, were employed as the supporting electrolyte. The desired solution pH was adjusted by different amounts of 10 mM Na_2HPO_4 and NaH_2PO_4 solutions. Pure water was used throughout, which was obtained using a Millipore Q water purification apparatus with resistivity over 18 MΩ cm.

Poly(allylamine) ferrocene (Fc-PAH) was synthesized according to the literature.[5] Approximately 16 mg of ferrocene carboxaldehyde was dissolved in 10 mL of methanol and added dropwise within an hour to 60 mL of an anhydrous methanolic solution of 80 mg of poly(allylamine) containing 0.52 mL of triethylamine. The mixture was stirred for another hour at room temperature, then sodium borohydride was carefully added in portions at 0 °C, and stirring continued for 90 min, finally the mixture was dried in vacuum at 35 °C, and the residue was extracted with distilled water. The aqueous solution was further purified by membrane dialysis against water.

2.2. Instruments. Cyclic voltammetry and chronamperometry measurements were carried out on CHI 600 and CHI832 electrochemical workstations (CH Instruments, USA), respectively. A conventional three-electrode setup was used. The MWNT/GOx-modified electrode was used as the working electrode. Coiled platinum wire and a Ag/AgCl (saturated KCl) electrode were used as the counter electrode and the reference electrode, respectively. The PBS was purged with high-purity nitrogen for at least 30 min prior to experiments, and a nitrogen atmosphere was then kept over the solution in the cell. The chronamperometry measurements of glucose were performed in a N_2 saturated solution at constant potential under stirring. Electrochemical impendence spectroscopy measurements were performed in the same electrochemical cell with a PARC M398 electrochemical impedance system (EG & Princeton Applied Research, Princeton, NJ) consisting of a potentiostat model 273 and a computer-controlled PAR model 5210 lock-in amplifier with EG &G AC impedance software, scanning from 10 kHz to 1 Hz-. Fluorescence emission spectra of GOx deposited in multilayer films were recorded by LS 55 spectrofluorometer using a Xe arc lamp and single-grating monochromators for excitation and emission. Transmission electron microscopy (TEM) measurements were made on a JEOL 2010 transmission electron microscope operated at an accelerating voltage of 200 kV. X-ray photoelectron spectroscopy (XPS) measurements were conducted with an ESCLAB MK II spectrometer (VG Co.) with Mg KR radiation as the X-ray source.

2.3. Preparation of Fc-PAH@CNT and $(Fc\text{-}PAH@CNT/GOx)_n$/$ITO)_n$ Multilayer Membranes. CNTs (0.5 mg) were solubilized in 1 mL of Fc-PAH solution (pH 7.0) with a 30 min sonication. The mixture was then centrifuged at 10 000 rpm for 15 min to separate Fc-PAH@CNT from the supertant. The nanotubes were redispersed in pH 7.0 buffer and centrifuged, and the supernatant was discarded. This redispersion/centrifugation cycle was repeated two additional times to ensure removal of all of the unabsorbed Fc-PAH from the Fc-PAH@CNT. ITO glass plates with dimensions of 7 mm × 30 mm were cleaned by ultrasonication in a series of solvents, Milli-Q water, ethanol, and ethanol aqueous solution saturated with NaOH, to provide a clean, negatively charged surface. The negatively charged substrate ITO was first immersed in PDDA aqueous solution (2 mg mL^{-1}) and PSS aqueous solution (2 mg mL^{-1}) for 15 min each. After being washed with distilled water, the Fc-PAH@CNT/GOx bilayers were grown on the PSS-terminated film by alternately dipping the modified ITO electrode into the Fc-PAH@CNT solution (0.5 mg mL^{-1}) and GOx solution (pH 7.0) for 20 min respectively. The membranes were carefully washed with distilled water for $n \times 5$ min (n is the number of layers). This sequence was repeated until the desired number of Fc-PAH@CNT/GOx bilayers was obtained.

2.4. Detection of the Amount of GOx Deposited in the $(Fc\text{-}PAH@CNT/GOx)_n$/ITO Electrode. The amount of GOx immobilized on the electrode surface was estimated by measuring the fluorescence intensity of FAD, which is known to be present as the redox centers 2 mol of 1 mol of GOx molecules.[17a,b] Since the fluorescence intensity of FAD bound to apo-GOx is weak, it was desired to obtain measurements of FAD on its release from GOx.[17c,d] For this purpose, the $(Fc\text{-}PAH@CNT/GOx)_n$/ITO electrodes were soaked in 2 mL of 8 mol mL^{-1} urea solution under agitation for 2 days under a N_2 atmosphere in the dark. The fluorescence intensity of the resulting solution was measured at 530 nm with excitation at 400 nm, and the amount of the immobilized GOx was evaluated using a calibration curve between the concentration of FAD and the fluorescence intensity, which was obtained by dissolving commercially available FAD into 8 mol mL^{-1} urea solution for concentrations smaller than 1.0×10^{-7} mol mL^{-1}. The 2 day soaking of the electrode in the urea solution seemed enough to release FAD from GOx as already reported because no change in the fluorescence intensity was observed for more than 2 days, as long as the solution was stored in the dark under N_2 atmosphere.[17]

3. Results and Discussions

3.1. Characterization of Fc-PAH@CNT Nanohybrids. The key to the formation of Fc-PAH-modified CNTs is the interaction between Fc-PAH and CNT, because the interactions between PAH and CNT are assumed to be dominated by Coulomb interactions,[18] so the electrostatic interaction is strongly influenced by the electrolyte concentration and by the solution pH. There are several factors that should be taken into account. As reported by Sigmund,[18] the adsorption competition between Na^+ ions and polycations will affect the stability of the complex

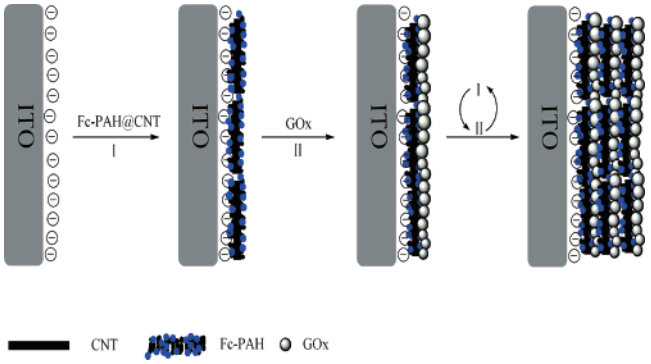

Figure 1. Schematic structure of the multilayer membranes.

of shortened MWNTs- and polyelectrolyte. According to the titration of PAH[19] the free energy of protonation to the fully unprotonated polymer increases as the pH of the solution increases. In addition the enzyme activity is also pH-dependent; the optimal pH of GOx is around 7.0 for the charge distribution on the enzyme surface and might be changed in the unique microenvironment.[20] Therefore, we chose to work at pH 7.0 adjusted by 10 mM Na_2HPO_4 and NaH_2PO_4 solutions. The isoelectric point of shortened MWNTs is around pH 2[18] therefore CNTs will be charged negatively when dispersed in pH 7.0 solutions. At pH 7.0, 85%[21] of the amine groups in the PAH are protonated, so the polymer carries enough positive charge to realize the interaction between PAH and CNTs. It has been established theoretically[49] and experimentally[50,51] that amine groups possess significant affinity for physisorption along the SWNT sidewalls, so we considered these factors also to contribute to the formation of Fc-PAH@CNT. As shown in Figure 1, the Fc-PAH could associate with the sidewall surface of CNTs, resulting in positively charged Fc-PAH-modified CNTs. The formed Fc-PAH-modified CNTs are stable for more than 2 weeks when dispersed in pH 7.0 PBS. The formation of this nanohybrid was further characterized by XPS as shown in Figure 2; the XPS spectrum of the Fc-PAH@CNT exhibits the Fe 2p3/2, Fe 2p1/2, and N 1s peaks with binding energies of 711.6, 724.5, and 400.65 eV, respectively, which are typically characteristic of Fe and N. These observations confirm the attachment of Fc-PAH onto the CNT. Moreover, the cyclic voltammogram obtained with the Fc-PAH@CNT confined on the ITO electrode gives a pair of well-defined redox peaks of ferrocene with $E^0 = 342$ mV vs Ag/AgCl in 10 mM PBS (pH 7.0), indicating that Fc-PAH can be associated with the sidewalls of CNTs. The value of E^0 is 57 mV more negative than the original Fc-PAH-modified ITO in the same electrolyte. This is probably due to some Fc redox centers covalently attached to the PAH adsorption on the CNT surface by the interaction of $\pi-\pi$ stacking,[22] this electron-drawing effect results in the negative shift of E^0. While an electrostatic Donnan effect may also ascribe to this phenomenon. The separation between the anodic and cathodic peak potential (ΔE_p) for Fc-PAH@CNT/ITO at a scan rate of 20 mV s^{-1} is 32 mV, which is larger than that of Fc-PAH/ITO (ca. 21mV at 20 mV s^{-1}), suggesting that the interactions between CNT and Fc-PAH restrict the mobility of the polymer backbone and the redox centers. Similar results were obtained for Fc encapsulated inside the SWNTs in the aqueous solution[22] and other redox polymer−SWNT systems.[23] Despite the interaction between Fc and CNTs, the reversibility of the voltammetric responses in aqueous solution for this Fc-PAH@CNT nanohybrid is highly improved, as compared with those of other Fc-modified CNT nanomaterials. Unlike the Fc-PAH/ITO electrode whose peak current decreases rapidly,

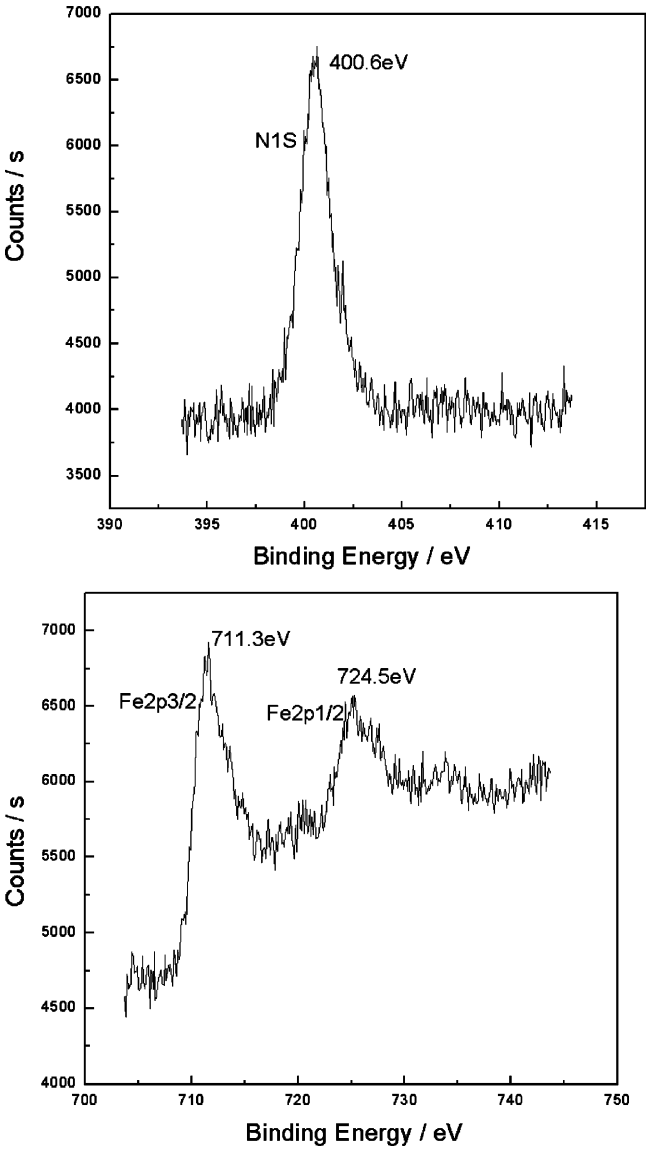

Figure 2. X-ray photoelectron spectra of N 1s and Fe 2p energy levels of Fc-PAH@CNT nanohybrids.

the peak currents of Fc-PAH@CNT/ITO electrodes decrease slowly during electrochemical scanning; when Fc-PAH@CNT/ITO was scanned continuously for 400 cycles at 100 mV s^{-1} this resulted in peak currents decreasing less than 5%. The stable Fc-PAH@CNT/ITO should have better performance in its practical applications.

3.2. SEM Characterization of Fc-PAH@CNT/GOx Multilayer Electrodes. The isoelectric point of native GOx in water is 4.05,[24] so the enzyme is negatively charged at neutral pH and can be electrostatically adsorbed onto positively charged Fc-PAH@CNT-modified surfaces. Randomly oriented CNTs could be seen from the SEM image of the obtained Fc-PAH@CNT layer (Figure 3A). The CNTs uniformly covered the surface of the ITO electrode. The density of CNTs in the first bilayer was rather small, but the individual carbon nanotubes were interweaved and homogeneously integrated with Fc-PAH without any sign of phase segregation. In particular, most of the CNTs were very different from the bundles,[25,26] indicating that this method was efficient to form a well-dispersed CNT layer. The glucose oxidase molecules could be deposited on the Fc-PAH@CNT layer by immersing the Fc-PAH@CNT-modified ITO electrode in pH 7.0 PBS containing 1 mg mL^{-1} GOx. A saturated enzyme layer could be formed after 20 min.

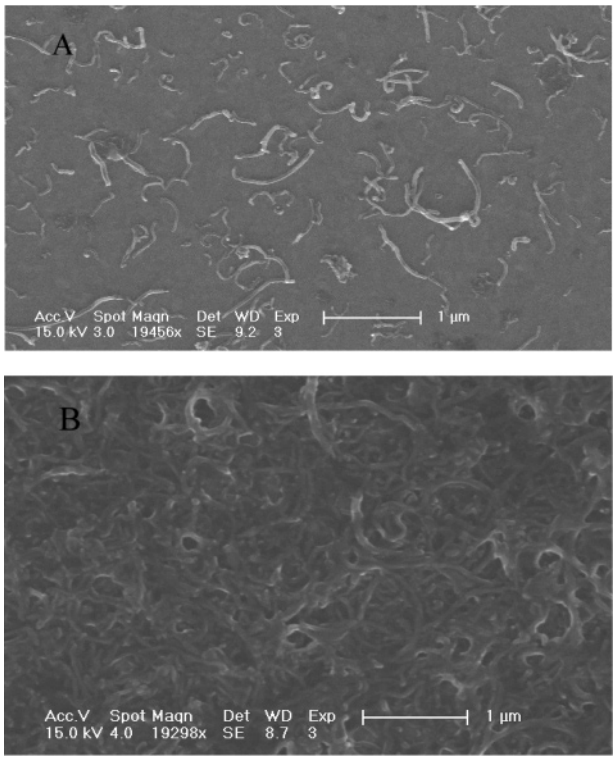

Figure 3. Scanning electron micrographs of (A) Fc-PAH@CNT and (B) $(Fc\text{-}PAH@CNT/GOx)_5$ films on ITO surfaces.

As shown in the SEM image (Figure 3B), GOx molecules were aggregated on CNTs due to the large surface-to-volume ratio of CNTs. As a result, the nanotubes became "fat". The sequential repetition of the deposition of Fc-PAH@CNT and enzyme could produce a multilayer membrane with a porous structure, which would be favorable for the approach of substrates to the enzyme molecules in internal layers. In addition to the SEM characterization, evidence for the uniform deposition of Fc-PAH@CNT/GOx bilayers was obtained from electrochemical analysis; it can be concluded that this porous and three-dimensional nature of the multiplayer films consisted of homogeneously dispersed CNTs by the LbL method.

3.3. Electrochemical Properties of $(Fc\text{-}PAH@CNT/GOx)_n$ Electrodes. It has been reported that LbL films containing Fc residues exhibit a redox response when being deposited on the surface of the electrode.[5] Figure 4A depicts cyclic voltammograms (CVs) of a $(Fc\text{-}PAH@CNT/GOx)_5$ film-coated electrode measured in 10 mM PBS (pH 7.0); a linear increase of the anodic peak current with scan rate was observed as shown in the inset of Figure 4, which shows the characteristic surface-confined waves. When returning to the variation in the electrochemistry as we build up the successive layers, we observed a number of interesting trends: First, the peak separation between the anodic and the cathodic peaks (ΔE_p) depends on the number of bilayers; the ΔE_p value for the Fc-PAH@CNT/GOx film-coated electrode is 46 mV at 20 mV s^{-1}, whereas the value is 85 mV for $(Fc\text{-}PAH@CNT/GOx)_5$ film-coated electrodes. With the number of $(Fc\text{-}PAH@CNT/GOx)_n$ bilayers increased, the redox reaction is becoming apparently diffusion-controlled. Second, we note that the redox properties depend on the type of the outermost layer. The electrical charge density consumed during the oxidation of Fc to Fc^+ for the $(Fc\text{-}PAH@CNT/GOx)_n$ Fc-PAH@CNT film-coated electrodes is increased by about 4 μC cm^{-2} when the outermost surface of the electrodes is covered with GOx. This could arise either through loss of Fc-PAH@CNT to the enzyme solution or through some of the ferrocene groups becoming non-

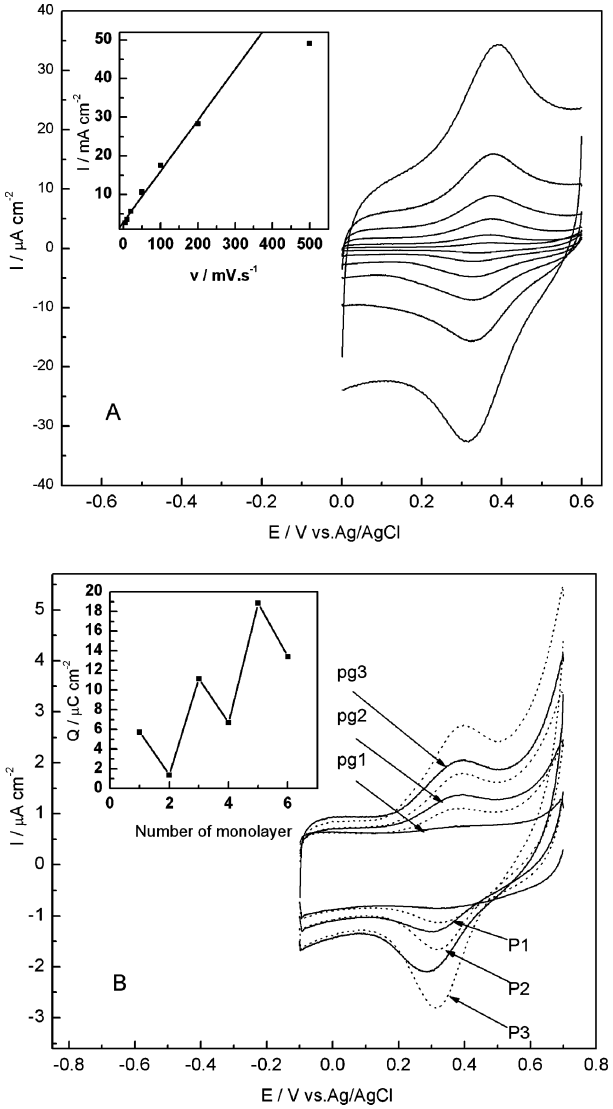

Figure 4. (A) Cyclic voltammograms for an electrode for five Fc-PAH@CNT/GOx bilayers at sweep rates of 10, 20, 50, 100, 200, and 500 mV s^{-1} in pH 7.0 10 mM buffer. Inset: Dependence of the anodic peak current (a) with potential sweep rates and (b) their square roots. (B) Cyclic voltammograms of self-assembled Fc-PAH@CNT/GOx multilayers in 10 mM PBS at pH 7.0. p1, p2, and p3 correspond to Fc-PAH@CNT-terminated layers, and pg1, pg2, and pg3 are GOx-terminated layers. The sweep rate was 20 mV s^{-1}. Inset: Dependence of integrated charge of CV for different monolayers of the self-assembled multilayer Fc-PAH@CNT/GOx electrode.

redox-active following adsorption of the enzyme onto the polymer. The higher response of the cationic PAH-terminated film may be ascribed in part to the facilitated anion transport through the film to compensate for the positive charges of ferricinium cations.[27] In other words, the redox activity of the films depends on the polarity of the electric charges on the outermost surface of the film, which is often the case for redox-active LBL films.[5,11,26,39] However, despite this effect there is a steady increase in the amount of redox-active ferrocene on the electrode for each successive Fc-PAH@CNT/GOx bilayer added. Third, there is an increase in both the background and the peak currents. The fact that the background voltammetric response increased for the CNT-modified electrode is not surprising since similar effects for CNT films cast on electrodes have been reported by others[6] and are most likely due to a larger electrode area undergoing double-layer charging and background reactions.

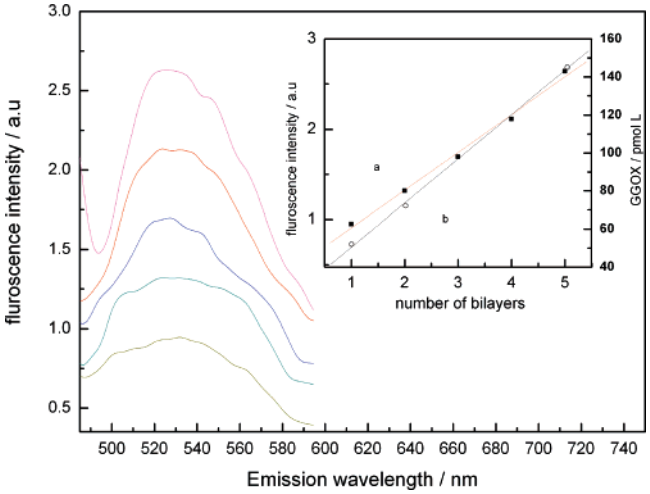

Figure 5. Fluorescence emission spectra of $(Fc\text{-}PAH@CNT/GOx)_n$ bilayers with different numbers. From the lower to upper curves, the number of Fc-PAH@CNT/GOx bilayer is 1, 2, 3, 4, and 5. Inset: Plots of the (a) intensity at 530 nm and (b) surface coverage of GOx vs the number of Fc-PAH@CNT/GOx bilayers.

3.4. Determination of the Amount of GOx Deposited in the Fc-PAH@CNT/GOx Multilayer Films by Fluorescence Spectroscopy. Fluorescence spectroscopy was employed to follow the deposition process of the multilayer films.[17a] The $(Fc\text{-}PAH@CNT/GOx)_n$/ITO electrodes were soaked in 2 mL of 8 mol mL^{-1} urea solution with agitation for 2 days under a N_2 atmosphere in the dark for FAD release from GOx. FAD is known to be present as the redox centers as 2 mol for 1 mol of GOx molecules. Assuming that the fluorescence intensity is proportional to the concentration of GOx, the buildup of the multilayer films can be estimated from fluorescence measurements. Figure 5 shows the fluorescence spectra of the multilayer films with a different number of layers. It is clear that the multilayer fluorescence intensity of the Fc-PAH@CNT/GOx assemblies is reproducible with sequential deposition. The strong band (530 nm) increases linearly with the number of deposited Fc-PAH@CNT/GOx bilayers with a correlation coefficient of 0.998 (Figure 5a), suggesting that the Fc-PAH@CNT nanohybrid can form LBL films with GOx, and the amounts of GOx adsorbed in each bilayer were almost the same. Thus, the amount of deposited materials simply could be controlled by selecting the number of bilayers. On the basis of the calibration curve, the loading of GOx (Γ) in the film could be obtained. Γ in the first Fc-PAH@CNT/GOx bilayer is 52 pmol cm^{-2}; with the increase of the bilayers a linear increment of the coverage of enzyme per bilayer was estimated (curve b in the inset of Figure 5).

3.5. Biocatalytical Performance of the $(Fc\text{-}PAH@CNT/GOx)_n$/ITO Electrodes to Glucose. We consider the double-redox-enzyme catalytic cycle for the oxidation of glucose (S) to gluconic acid (P), catalyzed by GOx and mediated by Fc-PAH@CNT nanohybrids as depicted as follows[28,29]

$$\text{Fc-PAH} \rightarrow \text{Fc}^+\text{-PAH} + \text{e}^- \quad (1)$$

$$2\text{Fc}^+\text{-PAH} + \text{GOx(FADH}_2) \xrightarrow{K} 2\text{Fc-PAH} + \text{GOx(FAD)} + 2\text{H}^+ \quad (2)$$

$$\text{GOx(FAD)} + \text{S} \overset{K_m}{\longleftrightarrow} \text{GOx(FAD-S)} \xrightarrow{K_{cat}} \text{GOx(FADH}_2) + \text{P} \quad (3)$$

Reaction 1 takes place at the ITO surface, charge transport between suitably positioned ferrocene sites in the polymer through CNTs that are in contact with the underlying negatively charged surface. The ping-pong enzyme kinetics of glucose oxidase are described by reactions 2 and 3.[30] Reaction 3 describes the Michaelis−Menten kinetics for the oxidation of glucose by GOx (FAD). In the absence of the diffusion of glucose in the thin self-assembled layered structure, the expression for the catalytic glucose oxidation current density is[31]

$$I_{cat} = \frac{2Fk_{cat}\Gamma_{ET}}{1 + \frac{k_{cat}}{k[\text{Fc}^+]} + \frac{k_M}{[\text{S}]}} \quad (4)$$

The Michaelis constant for glucose is $K_M = (K_{-1} + K_{cat})/K_1$, and K_{cat} and K, respectively, are the enzyme turnover and the bimolecular $FADH_2$ reoxidation rate constant (wiring efficiency). Γ_E is the surface concentration of the total active enzyme. Figure 6A shows CVs for electrode located with 1−5 Fc-PAH@CNT/GOx bilayers in a solution containing 0.5 mM

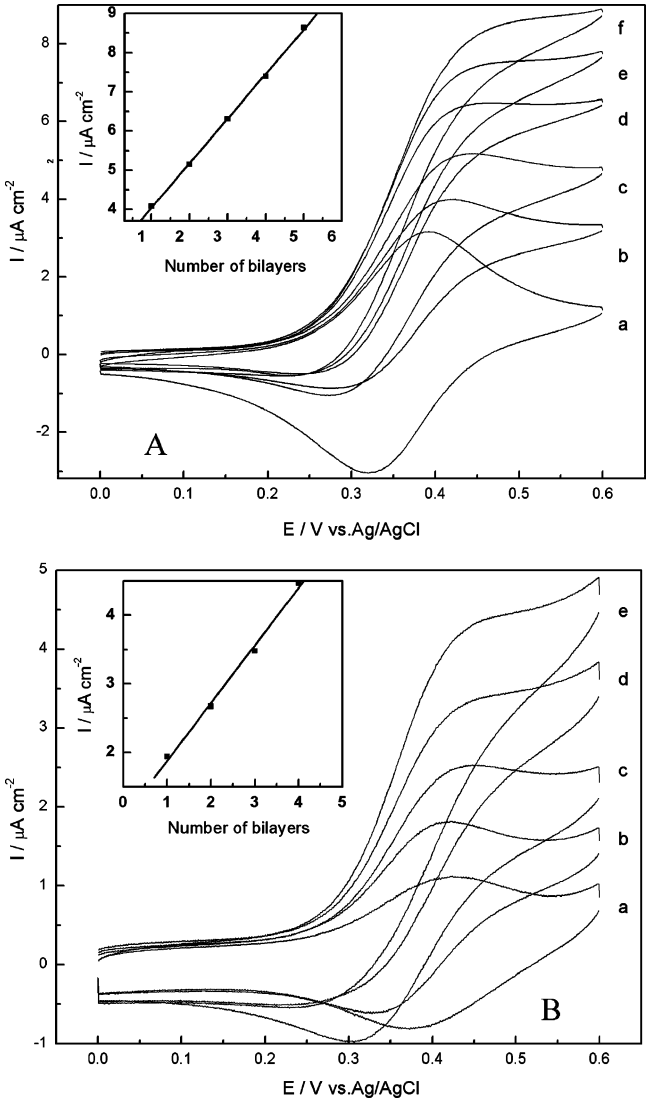

Figure 6. (A) Cyclic voltammograms of (Fc-PAH@CNT/GOx)-modified ITO electrodes in pH 7.0 10 mM PBS in the (a) absence and (b−f) presence of 0.5 mM glucose. The *n* denotes the number of Fc-PAH@CNT/GOx bilayers, n = (b) 1, (c) 2, (d) 3, (e) 4, (a and f) 5. Sweep rate: 20 mV s^{-1}. Inset: Catalytic current vs the number of Fc-PAH@CNT/GOx bilayers. (B) Cyclic voltammograms of Fc-PAH/GOx-modified ITO electrodes in the same condition, n =(a and b) 1, (c) 2, (d) 3, (e) 4. Inset: Catalytic current vs the number of Fc-PAH/GOx bilayers.

glucose under N_2 atmosphere. As the potential increases the ferrocene within the films is oxidized to ferricinium, and we observe a catalytic current for the oxidation of glucose. As can be seen from the inset of Figure 6, the anodic peak currents showed a linear dependence on the number of bilayers. Thus, it is considered that every bilayer contains the same amount of active enzyme, which could be calculated by eq 4, and the Fc-PAH@CNT/GOx multilayers are constructed in a spatially ordered manner; this anticipation was also confirmed by the fluorescence measurements, as shown in Figure 5. For comparison, multilayers of Fc-PAH/GOx were assembled on an ITO electrode (termed $(Fc\text{-}PAH/GOx)_n$/ITO) by LbL self-assembly of Fc-PAH and GOx, and the cyclic voltammetric responses of this enzyme-modified ITO electrode in the presence of glucose are shown in Figure 6B. It can be seen that I_{cat} slowly increased with the number of Fc-PAH@CNT/GOx bilayers. For four-layer GOx depositions, I_{cat} was only 4.82 μA cm^{-2} when 1 mM glucose was added, while for the $(Fc\text{-}PAH@CNT/GOx)_4$/ITO, for only 0.5 mM glucose, the I_{cat} was as high as 7.33 μA cm^{-2} at 460 mV vs Ag/AgCl. Figure 7A shows the steady-state current−time response of $(Fc\text{-}PAH@CNT/GOx)_4$-modified ITO electrodes at an applied potential of 0.5 V to glucose under N_2 atmosphere. The sensitivity calculated from the linear range of the concentration dependence of catalytic current (Figure 7B) was 5.08 μA mM^{-1} glucose cm^{-2} for $(Fc\text{-}PAH@CNT/GOx)_1$/ITO electrodea and increased to 30.8 μA mM^{-1} glucose cm^{-2} for the $(Fc\text{-}PAH@CNT/GOx)_4$/ITO electrodes. This result clearly shows that the sensitivity of the $(Fc\text{-}PAH@CNT/GOx)_n$ film-coated electrodes can be adjusted by modulating the deposition number of Fc-PAH@CNT/enzyme bilayers; the ability to control the sensitivity of the electrode should be useful, especially for the electrodes containing multiple enzymes with significantly different activities.

If $E \geq E^0$, then all ferrocene sites in the polyelectrolyte film are oxidized, and the electrocatalytic current for the oxidation of glucose depends on the concentration, as shown in Figure 7B; the best fit to eq 4 is shown by the solid line, where we replace $[Fc^+]$ by $[Fc]_{TOT}$ because we are in the limiting current region. If the film thickness (d_f) of 50 nm per bilayer obtained by SEM observation is used, which led to the Fc site concentration, then $[Fc] = Q/(FAd_f)$.[33] Substituting in estimates for K_m and K_{cat} of 25 mM and 700 s^{-1} from the literature,[32] the value of the molecular wiring efficiency is the $FADH_2$ bimolecular reoxidation rate constant, K, which can readily be obtained from K[Fc] once the volume concentration of mobile polymer-bound Fc sites colliding with the active enzyme $FADH_2$ is evaluated. The resulting values of K[Fc] and Γ_{ET} are compared in Table 1. As shown in Table 1, the K values are almost independent of the film thickness of the $(Fc\text{-}PAH@CNT/GOx)_n$ electrodes; this is due to the flux of electrons that can reoxidize the enzymatic $FADH_2$ in the GOx layers further away from the underlying electrode surface, which is limited by the diffusion-like propagation of electronic charge in the self-assembled multilayers.[11] A similar phenomenon was observed in (Os-PAH-Os/GOx) multilayers.[48] The bimolecular $FADH_2$ oxidation rate constant K is 12-fold higher than the rate constants reported previously by Hodak.[5]. The process of enzyme $FADH_2$ oxidation by the artificial redox mediator undergoes three main steps: (i) diffusion of the redox mediator to the enzyme surface, (ii) suitable positioning with the respect to the prosthetic group, (iii) electron transfer from the $FADH_2$ to the mediator. In the present case, the Fc's are covalently attached to the polymer backbone, and the later two steps are the decisive steps. Due to the anisotropy for the electron-transfer process in the $FADH_2$ oxidation by the redox polymer, only a fraction of redox mediator that approaches the enzyme surface at an optimum orientation leads to efficient electron transfer. The spatial distribution of Fc-PAH-modified CNTs and GOx within the self-assembled structure can be significantly changed by varying the pH used during the self-assembly process. The use of high pH not only allows the incorporation of more Fc-modified polymer and enzyme but also enhances the [Fc]/[GOx] ratios.[40] The lager the ratio of Fc to the total GOx concentration, the greater the fraction of wired enzyme, since the greater fraction of Fc can be positioned at the enzyme surface with proper distance to the $FADH_2$ moiety.[41] In addition, the CNTs play a dual significant role in both the enzyme immobilization and

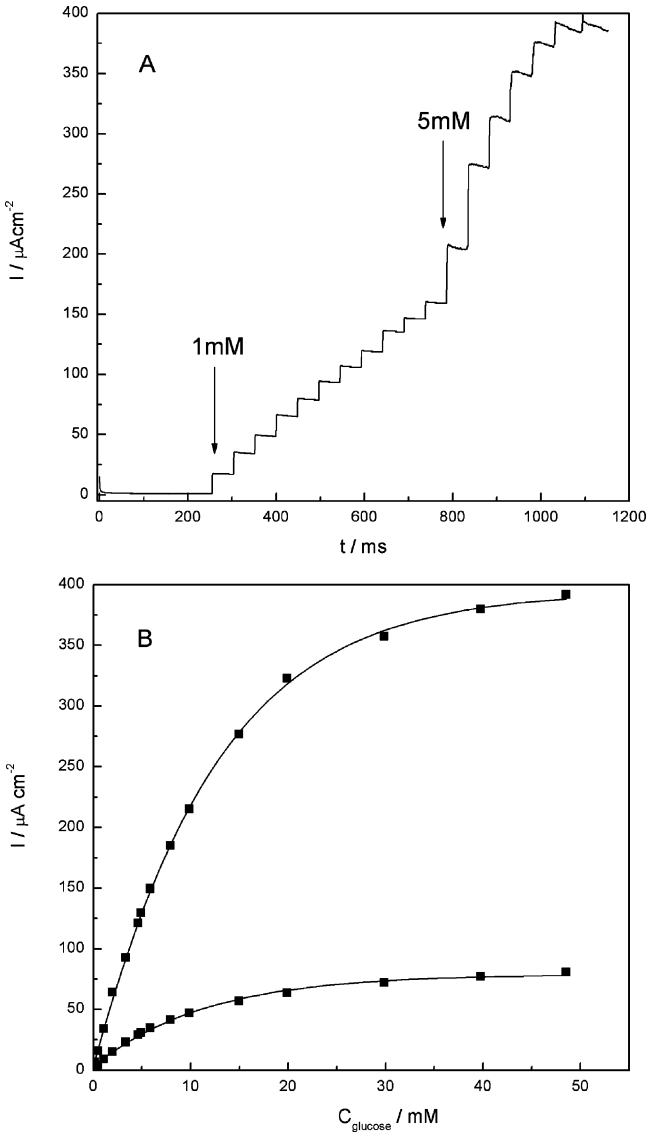

Figure 7. (A) Steady-state current−time response of $(Fc\text{-}PAH@CNT/GOx)_4$-modified ITO electrodes at an applied potential of 0.5 V to successive addition of 1 or 5 mM glucose in a stirred 10 mM PBS at pH 7.0 under N_2 atmosphere. (B) Glucose concentration dependence of the catalytic current at E = 0.5 V. Solid line best-fit curve corresponding to eq 4.

Table 1. Wiring Efficiency and Amount of Enzyme Wired[a]

experiments	K [Fc] (s^{-1})	Q (μC cm^{-2})	K (M^{-1} s^{-1})	Γ_{ET} (pmol cm^{-2})	Γ_{GOx} (pmol cm^{-2})
A	2672	19.69	2.6×10^5	6.0 (11.5%)	154
B	538	1.38	1.8×10^5	1.76 (1.1%)	52

[a] A and B correspond to four and one multilayers, respectively.

the transduction events, namely, as carriers for GOx to provide a suitable microenvironment to retain the GOx activity and as a transducer for amplifying the electrochemical signal of the product of the enzymatic reaction. According to the literature,[34] the enzyme becomes partially unfolded when associated with nanotubes; the tunneling distance of the optimum electron-transfer pathway[44] from the isoalloxazine group in the GOx to a cystamine residue C164 at the enzyme surface maybe reduced, which allows for improved access to the FAD centers by the Fc redox centers. Following the Marcus Theory,[45] the bimolecular $FADH_2$ oxidation rate coefficient is a negative exponential with the electron-transfer pathway distance; the greater wiring efficiency arises from the shorter tunneling distance. And the increased working electrode area provided by CNTs allowed for more of the redox polymer's ferrocene centers to be accessible.[27] Otherwise the nanostructure films generally have better catalytic efficiencies than the polyelectrolyte layers.[35] Assuming that the diameter of the Fc-PAH-functionalized CNT is 30 ± 5 nm, that of the GOx molecule is 7 nm.[43] Thus, it is possible that $(Fc\text{-}PAH@CNT/GOX)_n$ films have more "cavities" or "channels" than $(Fc\text{-}PAH/GOx)_n$ films. These channels may allow counterions in aqueous buffers to move into or out of the films more easily and greatly enhance the charge transport mobility within the films. More porous films would also allow the enzyme substrates to enter into the films more easily and have more chance to react with all of the proteins in the films, thus significantly improving the catalytic efficiency and the Γ_{ET}/Γ_{GOx} ratio as compared with the reported values, as shown in the Table 1. Turning to the values for Γ_{ET} in Table 1, we note that on going from one to four bilayers this parameter increases 4-fold as expected, and it is almost 30 times the literature-reported value.[5]

3.6. Electrochemical Impedance Characterization of the $(Fc\text{-}PAH@CNT/GOx)_n$ Membranes. Calvo and Wolosiuk performed a systematic study of the interdependence of structure and enzyme−electrode distance in "wiring efficiency" of self-assembled redox-active polyelectrolyte and enzyme multilayers.[11] They concluded that the generation of an electrical signal from the molecular recognition of glucose by GOx involves the following sequence of events: $FADH_2$ reoxidation, represented by $K_M = K[Os]$, and propagation of electrons from the active layer to the underlying electrode through the multilayers, K_D. Therefore, the observed rate of $FADH_2$ reoxidation, $K_{M(obs)}$, can be expressed as the sum of the reciprocals of the reoxidation rate K_M in the absence of electron propagation in eq 5[11]

$$\frac{1}{K_{M(obs)}} = \frac{1}{K_M} + \frac{1}{K_D} \tag{5}$$

where Δx is how redox charge propagates along the film a certain macroscopic distance. The diffusion characteristic time, τ, of this random walk can be related to D_e according to the well-known Einstein−Smoluchowski relation

$$\tau = \frac{\Delta x^2}{2D_e} \tag{6}$$

Combining eqs 5 and 6, we obtain eq 7

$$\frac{1}{K_{M(obs)}} = \frac{1}{K_M} + \frac{\Delta x^2}{D_e} \tag{7}$$

The electron diffusion coefficient can be determined by electrochemical impedance spectroscopy, At the redox polymer's formal potential, complex plane (Nyquist) impedance plots of

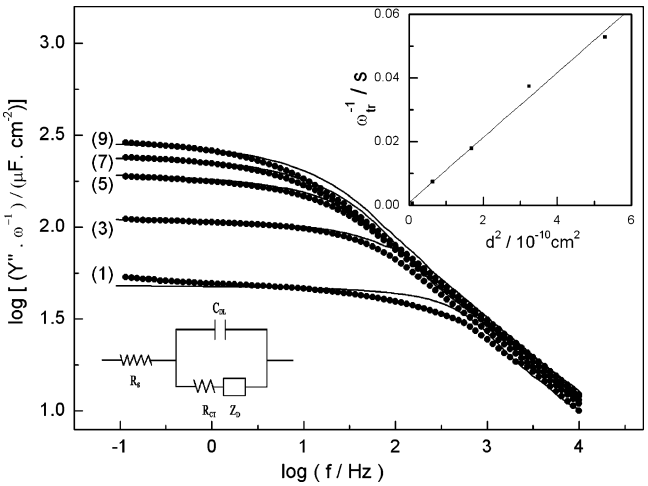

Figure 8. Log (Y''/ω) vs log(f) plots for an ITO electrode coated by $(Fc\text{-}PAH@CNT/GOx)_n$ (Fc-PAH@CNT) film in 10 mM PBS (pH 7.0), $E = 0.35$ V. The number at the left of each curve is the number of the adsorption steps ($2n + 1$). Solid lines represent the best fit of the circuit of the lower inset. Upper inset: Plot of ω_{tr}^{-1} vs d^2 to determine the apparent diffusion coefficient. From the fit, $D_{app} = 1.02 \times 10^{-8}$ cm^2 s^{-1}, $R^2 = 0.9953$. Lower inset: Equivalent circuit employed in study of the impedance spectra.

$(Fc\text{-}PAH@CNT)_n/GOx_m$ films show two distinct regions, as predicted by the finite transmission line model of Albery et al.[37] This behavior is consistent with those other redox polymer systems.[38] Fitting the spectrum to the equivalent circuit in the lower inset of Figure 8 yields large errors in the high-frequency areas. So we fitted only the high-frequency data with the Randles circuit; the value of R_{CT} derived from the first layer of the $(Fc\text{-}PAH@CNT/GOx)_5$ multilayer is 19 Ω; when the film was assembled with GOx, the R_{CT} increased by 18 Ω. Proceeding with the assembly of the multilayers, R_{CT} changed regularly, increasing when GOx assembled and decreasing when Fc-PAH@CNT assembled. It also agreed with the previous studies.[46] Calvo and Tagliazuccchi[39] have developed a model for electrochemical impedence spectroscopy (EIS) study of LbL self-assembly of redox polyelectrolyte multilayers; the diffusion process impedance is given by eq 8

$$Z_D(\omega) = -f(\eta)\frac{1}{C_F\omega}\left[\frac{\omega}{\omega_{tr}}\right]^{1/2} j^{1/2} \coth\left(\left[\frac{\omega}{\omega_{tr}}\right]^{1/2} j^{1/2}\right) \tag{8}$$

where Z_D is the finite diffusion impedance, ω is the angular frequency, C_F is the Faradaic capacitance, and $f(\eta)$ is the potential dependence as a function of apparent overpotential. The characteristic transition angular frequency ω_{tr} is defined as $\omega_{tr} = ((D_{app})/(d^2))$, where D_{app} is the apparent diffusion coefficient of charges in the film and d is the film thickness. The low- and high-frequency limits of the Faradaic capacitance (Y''/ω) are given respectively by

$$Y''/\omega(\omega \to 0) = -\frac{1}{f(\eta)} C_F \tag{9}$$

$$Y''/\omega(\omega \to \infty) = -\frac{1}{f(\eta)} \sqrt{2}\left(\frac{\omega}{\omega}\right)^{-1/2} C_F \tag{10}$$

Inspection of these equations indicates that it is possible to obtain quantitative information on the charge propagation that result from electron transport through the multilayer and movement of ions to compensate the electrical charges. The frequency dependence of the electrode capacitance for positively capped LbL $(Fc\text{-}PAH@CNT/GOx)_n$ multilayers is shown in Figure 8;

Table 2. Parameter Values Obtained by Fitting the EIS Data of Figure 8 to the Equivalent Circuit

layer	$C_{F,max}$ (μF cm^{-2})	ω_{tr} (Hz)
1	55	1111
3	108	156
5	183	59
7	230	31
9	278	19

the values for C_F and ω_{tr} that best fit the entire electrochemical impedance spectrum are shown in Table 2. For films with Fc-PAH@CNT as the outermost layer, the capacitance versus log(f) plots can be described by eq 8. We observe a shift of the transition frequency ($f_{tr} = \omega_{tr}/2\pi$) to lower values as more Fc-PAH@CNT layers are added. In the low-frequency region, the capacitance increases with the number of LbL multilayers. At very low frequency the capacitance increases versus log(f) for a small slope while eq 9 predicts a constant capacitance, which corresponds to the charge reaching the film−electrolyte interface with a pseudo-capacitive behavior. As the frequency increases, the capacitance decreases and reaches the common Warburg slope when electron transport becomes the limiting step for the propagation of charge. A similar behavior was observed in (Os-PAH/PVS) systems.[38] With the film thickness (d) determined as described earlier, the charge diffusion coefficient D_{app} may be found:[39] $\omega_{tr} = D_{app}/d^2$. The upper inset in Figure 8 shows a plot of the reciprocal of ω_{tr} versus the squared film thickness, which gave the value of the charge diffusion coefficient through this supramolecular structure of 1.02×10^{-8} cm^2 s^{-1}. This D_{app} value results from electron transfer between Fc sites tethered to the polymer backbone through CNTs and movement of ions to compensate for the electrical charges. It is anticipated that the diffusion coefficients of the supporting counterions ($H_2PO_4^-$, HPO_4^{2-}) used in our experiments with this supramolecular multilayer with a porous structure should be on the order of 10^{-5} cm^2 s^{-1}.[42] This estimate is much higher than the measured D_{app} value and suggested that D_{app} is the apparent electron diffusion coefficient (D_e) for electron propagation throughout the subsequent (Fc-PAH@CNT/GOx)$_n$ layers. However, since it is likely that the GOx layer was swollen in the electrolyte solution, the actual D_e value might be slightly larger than that estimated here. The D_e value obtained for (Fc-PAH@CNT/GOx)$_4$ (Fc-PAH@CNT) films are much higher than those for similar supramolecular architectures without the CNTs. The random distribution of redox centers on CNT surfaces yields a collection of clusters in which each molecule in a cluster is accessible by hopping between the molecules occupying adjacent sites. Here CNTs may perform as the "bridge" connecting two percolation clusters, and the electron transfer along the CNT is quite rapid, since CNTs are remarkably good conductors with long electron mean free paths.[47] The electron propagation among (Fc-PAH@CNT/GOx)$_n$ self-assembled nanostructures via bound diffusion of the redox molecules and electron hopping from one reduced molecule to an adjacent oxidized molecule[47] take place as long as the electron transfer along the CNT. So this redox-polymer-modified CNT nanohybrid could greatly facilitate the electron transport though LbL multilayers. In addition, the distances between redox sites of the enzyme and the electrode, the distances between the mediator and the electrode, and the electron-hopping distance between redox centers covalently attached to the polymer backbone were eliminated by the possibility of charge transport by tunneling processes. That is to say that the electron-transfer barrier through this supramolecular architecture is lower for a system that includes short CNTs as connectors. In virtue of the excellent performance of CNTs in this supramolecular architecture, within the multilayer a proportion of GOx molecules very efficiently wired the Fc-PAH@CNT (K[Fc] > K_{cat}), which shows possible applications in fabrication of a glucose biosensor or a biofuel cell.

4. Conclusion

A simple and convenient method of preparing a multilayered biosensing interface has been developed, based on the construction of eletrostatically self-assembled intelligent nanostructures on electrodes with GOx and Fc-PAH-modified CNTs. The as-assembled Fc-PAH@CNT/GOx multilayer films have been demonstrated to possess striking properties: The incorporation of CNTs modified by Fc-PAH into enzyme films results in a 6−10-fold increase in the sensor's bioelectrocatalytic response for the oxidation of glucose current output; for the fabrication of redox-polymer-modified CNTs and enzyme nanohybrids by regulating the number of deposited layers in a stepwise manner, we can control the amount of adsorbed enzyme as well as polymer mediator; therefore, the amperometric current output is promising for the efficient fabrication of microbiosensors. The $FADH_2$ oxidation bimolecular rate constant (wiring efficiency) was increased 12-fold, which could greatly facilitate the electron transport from the redox-active site through the mediator to the electrode surface. At the same time, the electron diffusion coefficient (D_e) of this nanostructure, given by impedance spectroscopy to be over 10^{-8} cm^2 s^{-1}, is dramatically higher than those systems without CNTs by at least a factor of 10, indicating that electron transport in the new supramolecular architecture is enhanced by incorporation of CNTs into redox polymer−enzyme systems. In addition the fraction of wired GOx is also increased; more GOx molecules are able to communicate with the Fc-PAH through CNTs. The electrical communication between the redox active site of the enzyme and the electrode surface is greatly improved by the coordination of the redox polymer and CNTs. The combination of the Fc-PAH and CNTs opened up a new avenue to overcome the electron-diffusion barrier to realize the goal of an assembled monolayer of totally wired enzymes. Currently, the miniaturized enzyme electrode in conjunction with biofuel cell and microchip technology attracts much attention; in this regard, the method developed here should make a significant contribution to the fabrication of microbiosensors and biofuel cells. Finally, the synthetic manipulation of the surface groups of redox-polymer-functionalized CNTs and biomolecules is expected to find wide application in the areas of biomimetic membranes and surface biofunctionlization as well as biological and chemical sensors.

Acknowledgment. The authors thank the National Science Foundation of China (Grant Nos. 20427003 and 30575004).

References and Notes

(1) Clark, L. C., Jr.; Lyons, C. *Ann. N. Y. Acad. Sci.* **1962**, *102*, 29.
(2) (a) Rajagopalan, R.; Heller, A. In *Molecular Electronics*; Jortner, J., Ratner, M., Eds.; Blackwell Science: Oxford, U. K., 1997; pp. 241. (b) Willner, I.; Katz, E. *Angew. Chem.* **2000**, *112*, 1230 and references therein. (c) Katz, E.; Willner, I.; Kotlyar, A. B. *J. Electroanal Chem.* **1999**, *479*, 64−68. (d) Barton, S. C.; Kim, H. H.; Bingaimin, G.; Zhang, Y.; Heller, A. *J. Am. Chem. Soc.* **2001**, *123*, 5802−5803. (e) Mao, F.; Mano, N.; Heller, A. *J. Am. Chem. Soc.* **2003**, *125*, 4951.
(3) Heller, A. *Acc. Chem. Res.* **1990**, *23*, 128.
(4) Katz, E.; Riklin, A.; Shabtai, V. H.; Willner, I. *Anal. Chim. Acta* **1999**, *385*, 45.

(5) Hodak, J.; Etchenique, R.; Calvo, E. J.; Singhal, K.; Bartlett, P. N. *Langmuir* **1997**, *13*, 2708.
(6) Joshi, P. P.; Merchant, S. A.; Wang, Y. D.; Schmidtke, D. W. *Anal. Chem.* **2005**, *77*, 3183.
(7) (a) Heller, A. *Acc. Chem. Res.* **1992**, *23*, 128. (b) Heller, A. *J. Phys. Chem.* **1992**, *96*, 3579. (c) Degani, Y.; Heller, A. *J. Am. Chem. Soc.* **1987**, *110*, 1285. (d) Degani, Y.; Heller, A. *J. Am. Chem. Soc.* **1988**, *110*, 2615. (e) Degani, Y.; Heller, A. *J. Am. Chem. Soc.* **1989**, *111*, 2357. (f) Gregg, B. A.; Heller, A. *Anal. Chem.* **1990**, *62*, 258.
(8) (a) Decher, G.; Hong, J. D. *Ber. Bunsen−Ges.* **1991**, *95*, 1430. (b) Decher, G. *Science* **1997**, *277*, 1232.
(9) Calvo, E. J.; Etchenique, R.; Pietrasanta, L.; Wolosiuk, A.; Danilowicz, C. *Anal. Chem.* **2001**, *73*, 1161.
(10) Calvo, E. J.; Battaglini, F.; Danilowicz, C.; Wolosiuk, A.; Otero, M. *Faraday Discuss.* **2000**, *116*, 47.
(11) (a) Calvo, E. J.; Danilowicz, C.; Wolosiuk, A. *J. Am. Chem. Soc.* **2002**, *124*, 2452. (b) Calvo, E. J.; Wolosiuk, A. *ChemPhysChem* **2005**, *6*, 43.
(12) (a) Britto, P. J.; Santhanam, K. S. V.; Ajayan, P. M. *Bioelectrochem. Bioenerg.* **1996**, *41*, 121−125. (b) Wang, J., Musameh, M. *Analyst* **2003**, *128*, 1382.
(13) (a) Luo, H. X.; Shi, Z. J.; Li, N. Q.; Gu, Z. N.; Zhuang, Q. K. *Anal. Chem.* **2001**, *73*, 915. (b) Liu, G. D.; Lin, Y. H. *Electrochem. Commun.* **2006**, *8*, 251.
(14) (a) Li, J.; Ng, H. T.; Cassell, A.; Fan, W.; Chen, H.; Ye, Q.; Meyyappan, M. *Nano Lett.* **2003**, *3*, 597. (b) Gooding, J. J.; Wibowo, R.; Liu, J. Q.; Yang, W. R.; Losic, D.; Shapter, J. G.; Hibbert, D. B. *J. Am. Chem. Soc.* **2003**, *125*, 9006. (c) Patolsky, F.; Weizmann, Y.; Willner, I. *Angew. Chem., Int. Ed.* **2004**, *43*, 2113.
(15) Ramanathan, K.; Bangar, M. A.; Yun, M.; Chen, W.; Myung, N. V.; Mulchandani, A. *J. Am. Chem. Soc.* **2005**, *127*, 496.
(16) Zhao, H. T.; Ju, H. X. *Anal. Biochem.* **2006**, *350*, 138.
(17) (a) Kuwabata, S.; Okamoto, T.; Kajiya, Y.; Yoneyama, H. *Anal. Chem.* **1995**, *67*, 1684. (b) Tsuge, H.; Mitsuda, H. *J. Vitaminol.* **1971**, *17*, 24. (c) Swoboda, B. E. P. *Biochem. Biophys. Acta* **1969**, *175*, 365. (c) Swoboda, B. E. P. *Biochem. Biophys. Acta* **1969**, *175*, 380.
(18) Kim, B.; Park, H.; Sigmund, W. M. *Langmuir* **2003**, *19*, 2525.
(19) (a) Suh, J.; Paik, H.; Hwang, B. K. *Bioorg. Chem.* **1994**, *22*, 318. (b) Yoshikawa, Y.; Matsuoka, H.; Br, N. *Ise. Polym. J.* **1986**, *18*, 242.
(20) Liu, Y.; Wang, M. K.; Zhao, F.; Xu, Z. A.; Dong, S. J. *Biosens. Bioelectron* **2005**, *21*, 984.
(21) Choi, J.; Rubner, M. F. *Macromolecules* **2005**, *38*, 116.
(22) Sun, N. J.; Guan, L. H.; Shi, Z. J.; Li, N. Q.; Gu, Z. N.; Zhu, Z. W.; Li, M. X.; Shao, Y. H. *Anal. Chem.* **2006**, *78*, 6050.
(23) Sun, N. J.; Guan, L. H.; Shi, Z. J.; Zhu, Z. W.; Li, N. Q.; Li, M. X.; Gu, Z. N. *Electronchem. Commun.* **2005**, *7*, 1148.
(24) Voet, J. G.; Coe, J.; Espstein, J.; Matossian, V.; Shipley, T. *Biochemistry* **1981**, *20*, 7182.
(25) (a) Mamedov, A. A.; Kotov, N. A.; Prato, M.; Guldi, D. M.; Wicksted, J. P.; Hirsch, A. *Nat. Mater* **2002**, *1*, 190. (b) Zhang, M.; Yan, Y.; Gong, K.; Mao, L.; Guo, Z.; Chen, Y. *Langmuir* **2004**, *20*, 8781.
(26) Olek, M.; Ostrander, J.; Jurga, S.; Mohwald, H.; Kotov, N.; Kempa, K.; Giersig, M. *Nano Lett.* **2004**, *4*, 1889.
(27) Sato, H. S.; Anzai, J. I. *Biomacromolecules* **2006**, *7*, 2072.
(28) Calvo, E. J.; Danilowicz, C.; Diza, L. *J. Electroanal. Chem.* **1994**, *369*, 279.
(29) Danilowicz, C.; Etchenique, R.; Calvo, E. J.; Diaz, L. J. *Anal. Chem.* **1996**, *68*, 4186.
(30) Barlett, P. N.; Pratt, K. F. E. *J. Electroanal. Chem.* **1995**, *397*, 61.
(31) (a) Bourdillon, C.; Demaille, C.; Moiroux, J.; Saveant, J. M. *J. Am. Chem. Soc.* **1994**, *116*, 10328. (b) Bartlett, P. N.; Pratt, K. F. E. *J. Electroanal Chem.* **1995**, *397*, 61.
(32) Wilson, R.; Turner, A. P. F. *Biosens. Bioelectron* **1992**, *7*, 165.
(33) Forzani, E. S.; Otero, M.; Perez, M. A.; Teijelo, M. L.; Calvo, E. J. *Langmuir* **2002**, *18*, 4020.
(34) (a) Liu, J. Q.; Paddon-Row, M. N.; Gooding, J. J. *J. Phys. Chem. B* **2004**, *108*, 24, 8460. (b) Zhao, Y. D.; Zhang, W. D.; Chen, H.; Luo, Q. M. *Anal. Sci.* **2002**, *18*, 939.
(35) Liu, H. Y.; Rusling, J. F.; Hu, N. F. *Langmuir* **2004**, *20*, 10700.
(36) Blauch, D. N.; Saveant, J. M. *J. Am. Chem. Soc.* **1992**, *114*, 3323.
(37) Albery, W. J.; Elliott, C. M.; Mount, A. R. *J. Electroanal Chem.* **1990**, *288*, 15.
(38) (a) Cameron, C. G.; Pickup, P. G. *J. Am. Chem. Soc.* **1999**, *121*, 11773. (b) Musiani, M. M. *Electrochim. Acta.* **1990**, *35*, 1665.
(39) Tagliazucchi, M. E.; Calvo, E. J. *J. Electroanal Chem.* **2007**, *599*, 249.
(40) Flexer, V.; Forzani, E. S.; Calvo, E. *J. Anal. Chem.* **2006**, *78*, 399.
(41) Calvo, E. J.; Wolosiuk, A. *ChemPhysChem* **2004**, *5*, 235.
(42) Bu, H. Z.; English, A. M.; Mikkelsen, S. R. *J. Phys. Chem. B* **1997**, *101*, 9593.
(43) Hecht, H. J.; Kalisz, H. M.; Hendle, J.; Schmid, R. D.; Schomburg, D. *J. Mol. Biol.* **1993**, *229*, 153.
(44) Alvarez-Icaza, M.; Kalisz, H. M.; Hecht, H. J.; Aumann, K. D.; Schomburg, D.; Schmid, R. D. *Biosens. Bioelectron.* **1995**, *10*, 735.
(45) Marcus, R. A.; Sutin, N. *Biochim. Biophys. Acta* **1985**, *811*, 265.
(46) Xu, Z. A.; Gao, N.; Shaojun Dong, S. J. *Talanta* **2006**, *68*, 753.
(47) Blauch, D. N.; Savéant, J. M. *J. Am. Chem. Soc.* **1992**, *114*, 3323.
(48) Calvo, E. J.; Danilowicz, C. B.; Wolosiuk, A. *Phys. Chem. Chem. Phys.* **2005**, *7*. 1800.
(49) Basiuk, E. V.; Basiuk, V. A.; Banuelos, J.-G.; Saniger-Blesa, J.-M.; Pokrovskiy, V. A.; Gromovoy, T. Y.; Mischanchuk, A. V.; Mischanchuk, B. G. *J. Phys. Chem. B* **2002**, *106*, 1588.
(50) Kong, J.; Dai, H. *J. Phys. Chem. B* **2001**, *105*, 2890.
(51) Debjit, C.; Izabela, G.; Fotios P. *J. Am. Chem. Soc.* **2003**, *125*, 3370.

BM061049L